AD-A184 393 NUMERICAL SIMULATION OF THE REVERSED FIELD PINCH(U) 1/1
UKAEA CULHAM LAB ABINGDON ENGLAND P PIPER 1987
UNCLASSIFIED CLM-P821 F G 20/9 NL

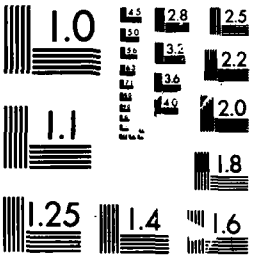

CLM-P803

NUMERICAL SIMULATION OF THE REVERSED FIELD PINCH

P. Kirby

Culham Laboratory, Abingdon, Oxfordshire, OX14 3DB, UK.

(EURATOM/UKAEA Fusion Association)

Abstract

This paper describes a series of numerical simulations of field reversal in the Reversed Field Pinch, using an incompressible MHD model and a reference set of plasma conditions. Field reversal and maintenance are observed, although at values of the pinch parameter θ larger than in experiment. This discrepancy is shown to arise largely from the unrealistic resistivity profile in the reference conditions and may not be fundamental. Qualitative agreement with experiment is demonstrated in several areas. The view that field reversal is due to a simple MHD dynamo is therefore given support.

(Submitted for publication in The Physics of Fluids)

November, 1986

Introduction

This paper describes the results from a series of numerical simulations of field reversal in the Reversed Field Pinch (RFP), using a cylindrical incompressible magnetohydrodynamic (MHD) model. The calculations presented here, the first in a program of numerical pinch modelling, apply specifically to the plasma conditions chosen in [1] as a basis for numerical comparison work.

The purpose of the paper is to record typical simulation results for simple macroscopic quantities of experimental interest and thus help assess to what degree single-fluid theory can explain the remarkable phenomenon of field reversal. These calculations extend those at present in the literature by providing a sequence of results rather than single instances of reversal.

The main feature of the present MHD model is the assumption of incompressibility. This was adopted as a physics choice as a particularly simple model with which to explore the hypothesis that field reversal is a gross electromechanical effect, not essentially altered by compressibility, transport etc.

The assumption of incompressibility also simplifies the numerical problem since magnetosonic waves and their severe timestep restrictions are absent from the system.

It should be noted that the plasma conditions taken from [1], notably the low value of Lundquist number S and the flat resistivity profile, are somewhat different from experiment. Furthermore, numerical simulation results are found to be fairly sensitive to the choice of resistivity profile. The results of this paper should therefore be clearly understood as applying to the numerical reference simulation proposed in [1], rather than an attempt to model precise experimental conditions.

With experiments in mind, the most obvious feature of the present results is the rather large value of pinch parameter θ required for reversal ($\theta \approx 2.3$). The result in [4] and preliminary results with the present code indicate that (even with an incompressible MHD model) at larger values of S and with a resistivity profile increasing towards the edge (nearer real conditions), the value of θ required for reversal drops to 1.4 - 1.6, much more consistent with experiment.

Background

Simulations of field reversal are not new and various simulation codes have been used during the development of the subject.

The first 3-dimensional numerical simulation of the pinch was that of Sykes and Wesson [2], using a compressible MHD model with anisotropic resistivity in cartesian geometry. This demonstrated field reversal and sustainment arising from gross MHD activity, but did not identify the precise dynamical processes responsible.

Park and Chu [3] used a 2-dimensional incompressible model with anomalous resistivity. Field reversal was obtained and a successful comparison made with the field profile in the eta-beta experiment.

Aydemir and Barnes [4] used a 3-dimensional incompressible MHD model with a resistivity profile increasing sharply at the plasma edge and obtained a steady reversed state with $\theta = 1.5$, $F = -0.03$ at $S = 5.10^3$.

Sato [5] has proposed a driven reconnection model of field reversal and has performed calculations with a compressible MHD model.

In [1], a comparison of field reversal calculations was undertaken using compressible and incompressible 3D MHD codes. This clearly demonstrated a difference between the compressible and incompressible results. For the single specific case run, the compressible codes gave field reversal whereas the incompressible codes did not. The macroscopic reason [1] for this difference appears to be a significant contribution of $\bar{v}_r \bar{B}_z$ to the $(\underline{v} \times \underline{B})_\theta$ term driving the j_θ current responsible for field reversal. (Here the bar denotes the axisymmetric part.) This contribution is identically zero in an incompressible fluid since $\bar{v}_r \equiv 0$. However, the contribution must also vanish at the reversal point ($\bar{B}_z = 0$) and therefore cannot be solely responsible for reversal, irrespective of the plasma model. The significance of this contribution and hence the degree of applicability of an incompressible MHD model awaits a more detailed comparison with experiment and a more detailed study of the results from compressible codes. There is no question, however, that field reversal can be obtained with an incompressible MHD model.

Numerical model

The numerical model [6] is that of single fluid incompressible MHD in a periodic cylinder. In dimensionless form the equations may be written

$$\frac{\partial \underline{v}}{\partial t} + \underline{v}.\nabla \underline{v} = -\nabla p + \underline{j} \times \underline{B} + \nu \nabla^2 \underline{v}$$

$$\frac{\partial \underline{B}}{\partial t} = \nabla \times \left(\underline{v} \times \underline{B} - \frac{\eta}{S} \underline{j}\right)$$

$$\nabla.\underline{v} = 0$$

$$\eta = \eta(r)$$

$$\nu = \text{const.}$$

Here, times are normalized to the Alfvén time based on the (minor) radius of the cylinder. S is the ratio of resistive diffusion time to Alfvén time and η is the resistivity profile. For the present case $S = 10^3$ and $\eta = 1$ [1]. The length of the cylinder is 2π (unit aspect ratio). Inclusion of the viscosity term is necessary to ensure non-linear numerical stability of the code. For the present case, it is sufficient to take $\nu = 10^{-4}$.

These equations are advanced in time using an explicit 2-step scheme with an implicit treatment of resistivity. A spectral method is used in the θ and z directions and conventional second order finite

differences in radius. Incompressibility is enforced by use of the standard MAC method. A detailed description of the code is available.

The boundary conditions are those pertaining to an impermeable, perfectly conducting, free-slip wall with a constant uniform driving electric field, i.e. $v_r = 0$, $B_r = 0$, $\omega_\theta = 0$, $\omega_z = 2v_\theta/r$, $E_\theta = 0$, $E_z = \text{const.}$ (Here $\underline{\omega} \equiv \nabla \times \underline{v}$.)

The initial magnetic field is taken to be the force-free equilibrium with safety factor profile q given by [1]

$$q(r) = 0.4\ (1.0 - 1.8748\ r^2 + 0.83232\ r^4).$$

(The field profiles are then obtained numerically.) This means that the initial conditions have a reversed B_z. It must be stressed that the simulations of field reversal described here are not a consequence of the choice of a reversed initial state. Field reversal is certainly obtainable starting from the more realistic case $B_z = \text{const.}$, which indeed is the initial condition normally used in the code. The initial velocity field is zero everywhere.

The equilibrium magnetic field is seeded with white noise at a relative level of 10^{-6} and the code run with $E_\theta = 0$ (constant 'toroidal' flux) and $E_z = \text{const.}$ for a substantial fraction of a field diffusion time. The value of E_z is chosen to give an appropriate value of the pinch parameter θ in the final state (and may therefore be different from that implied by the initial q profile).

The results described here were obtained using a modest computational mesh of $N_r = 32$, $N_\theta = 12$, $N_z = 25$. This means that poloidal mode numbers $0 \leq m \leq 3$ and toroidal mode numbers $-8 \leq n \leq 8$ are included in the calculations.

Results

Fig. 1 shows a typical plot of the pinch parameter θ and field reversal fraction F as a function of time. As the simulation proceeds the field rapidly loses the reversal of the initial state, but then suddenly reverses and remains marginally reversed for the remainder of the simulation, although with slight fluctuations. This remarkable behaviour is emphasized by the dashed lines showing how F and θ would evolve (under axisymmetric resistive diffusion) if there were no dynamo effect.

Fig. 2 shows F versus θ for the present plasma model (labelled $S = 10^3$ η = flat). It is obtained from a sequence of separate simulations (each like Fig. 1) with different values of the applied electric field E_z. Here and below we use the convention that each point on the graph is the time-averaged value in the respective quasi steady-state. The error bars then indicate the maximum deviation over time from this average. The diagram clearly demonstrates that field reversal can be obtained with an incompressible MHD model. However, for the present case, the value of pinch parameter θ required for reversal ($\theta \approx 2.3$) is larger than that observed in experiment ($\theta \approx 1.4$). This result and its known dependence on the choice of plasma conditions have been discussed above.

To illustrate this point, Fig. 2 also shows results obtained from a more realistic plasma model (labelled $S = 10^4$ η = shaped). This has a resistivity profile increasing towards the edge (the most significant change) and a larger S value. For this case, the $F - \theta$ curve lies considerably to the left of that for the present case of flat resistivity and is much more consistent with experiment. It is also consistent with the result in [4].

Fig. 3 shows the corresponding r.m.s. values of the relative fluctuation level $\delta B_\theta / B_\theta$ at the wall plotted against the driving electric field E_z. (Here $\delta B_\theta \equiv B_\theta - \bar{B}_\theta$.) The typical fluctuation level of $\simeq 10\%$, rather larger than the experimental value of $\simeq 1\%$, is also likely to be dependent on the choice of plasma conditions. Nevertheless, it is significant that the fluctuation level is not 100%, as might be expected from simplistic quasi-linear MHD scaling arguments. Whether MHD models always predict a relatively large level of fluctuation and thus whether a more complicated description is needed in this respect [7] can be decided only by further simulation work.

Fig. 4 shows the resistance per unit length (E_z/I) as a function of E_z. Shown for reference is the corresponding resistance obtained if the plasma acted as a solid conductor of the same resistivity. The clear non-linear relationship between the current and the applied voltage constitutes a numerical simulation of what is known experimentally as current 'screw-up'.

Fig. 5 shows simulation results for the μ profile (the ratio

$j_\parallel/B$) as a function of radius and makes a heuristic comparison with experimental values from the HBTX 1A experiment [8]. The simulation curve corresponds to the case of greatest reversal in Fig. 2 ($S = 10^3$, η = flat, $\theta \simeq 2.9$, $F \simeq -0.21$) and was calculated at the end of the run (time $t = 320$). It has a value of F nearest that of the experimental case. The experimental curve was obtained for $S \gtrsim 10^4$, $\theta \simeq 1.7$, $F = -0.3$, aspect ratio = 3 and is the only direct measurement of μ available from HBTX 1A. Although the differences in the cases preclude a true comparison, there is an encouraging consistency between the simulation and experimental results.

Fig. 6 shows the radial profile of the axisymmetric part of j_θ at the end of the calculation for the case $\theta \simeq 2.3$, $F \simeq 0$. Of fundamental physics interest is the macroscopic cause of this current, responsible for the decreasing $\bar{B}_z$ profile (through $\bar{j}_\theta = -\partial\bar{B}_z/\partial r$). To address this point, the axisymmetric parts of Ohm's law

$$\frac{\eta}{S}\bar{j}_\theta = \bar{E}_\theta + \langle(\underline{v} \times \underline{B})_\theta\rangle$$

are also displayed on the diagram. It is clear that $\langle v_z B_r\rangle$ is the principal driving term for the field reversal, $\langle v_r B_z\rangle$ is a minor contribution and $\bar{E}_\theta \simeq 0$. The importance of $\langle v_z B_r\rangle$ has also been suggested by Sato [5].

Fig. 7 shows a $\log_{10}$ plot of the energy spectrum (the energy in each Fourier harmonic) of B_r as a function of time for the case $\theta \simeq 2.3$, $F \simeq 0$. (For reference, the corresponding $\log_{10}$ energy spectrum value of

$\bar{B}_\theta$ is typically +0.1.) It shows the dominance of the two modes m = 1, n = -2 and m = 1, n = -3 throughout the simulation. (For simplicity of representation, only these modes have been labelled on the figure.) In general, the dominant modes are found to be resonant inside the reversed surface. The importance of m = 1 modes is consistent with experiment [9].

Fig. 8 shows the energy spectrum at the end of the same calculation (time t = 500) as a histogram in (m,n) space. It provides a simple picture of the amplitude of the various modes, in particular the non-linear m/n sequence 1/-2, 1/-3, 2/-5, 3/-8.

Concluding Remarks

3-dimensional numerical simulations of field reversal in the Reversed Field Pinch have been performed using (as a physics choice) the simplest incompressible MHD model and a reference set of plasma conditions [1]. Field reversal and maintenance are clearly observed. The F - θ curve has been presented.

There is considerable qualitative agreement between the numerical results (F - θ curve, fluctuation levels, fluctuation spectrum, current screw-up and μ profile) and experimental observations.

For the present case, the numerical values of the pinch parameter θ and fluctuation levels are rather larger than in experiment. However, this quantitative discrepancy is known to arise largely from the choice of

somewhat unrealistic plasma conditions, and may simply reflect the need for correspondingly increased MHD activity.

Taken together, these results lend weight to the view that field reversal is a phenomenon arising principally from single fluid MHD dynamo action.

In common with all previous work, the present simulations are essentially a series of macroscopic numerical experiments and do not attempt to identify the detailed nature of the modes responsible for the dynamo. Calculations are in hand to explore this question, to establish the results for more realistic S values, aspect ratios and resistivity profiles, and to make further comparisons with experiment.

Acknowledgement

It is a pleasure to acknowledge discussions with M.K. Bevir and C.G.Gimblett.

References

1. A.Y. Aydemir, D.C. Barnes, E.J. Caramana, A.A. Mirin, R.A. Nebel, D.D. Schnack, A.G. Sgro, Phys. Fluids 28 898 (1985).

2. A. Sykes, J.A. Wesson, Proc. 8th European Conference on Controlled Fusion and Plasma Physics, Prague Vol 1. p.80, (1977).

3. W. Park, C.K. Chu, Nuclear Fusion 17 1100 (1977).

4. A.Y. Aydemir, D.C. Barnes, Phys. Rev. Lett. 52 930 (1984).

5. T. Sato, K. Kusano, 10th International Conf. on Plasma Physics and Controlled Nuclear Fusion Research, London 1984, paper D-II-4-1.

6. P. Kirby, Proc. 11th International Conference on Numerical Simulation of Plasmas, Montreal, 1985, paper 2.B.08; Proc. 8th European Conference on Computational Physics, Eibsee, p.23, 1986.

7. A.R. Jacobson, R.W. Moses. Phys. Rev. Lett. 52 2041 (1984).

8. D. Brotherton-Ratcliffe, I.H.Hutchinson, Culham Laboratory Report CLM-R246 (1984).

9. I.H. Hutchinson, M. Malacarne, P. Noonan, D. Brotherton-Ratcliffe, Nuclear Fusion 24 59 (1984).

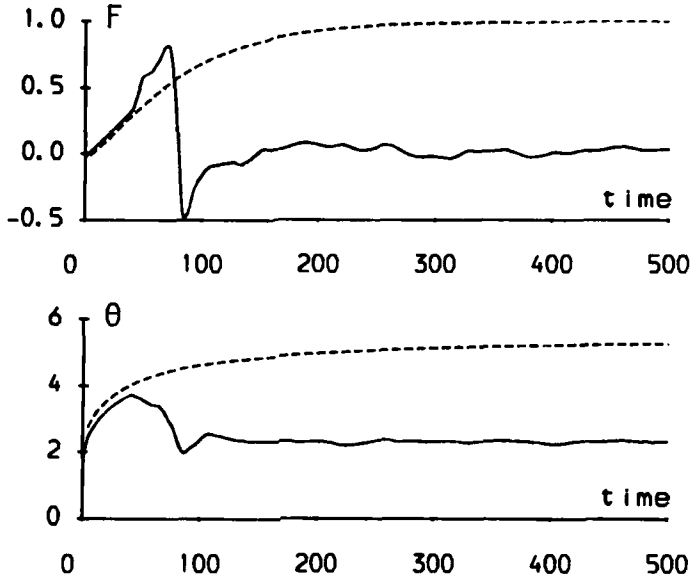

Fig.1 F and θ vs. time. Dashed lines show evolution under 1D resistive diffusion. (Case: S = 10^3, η = flat).

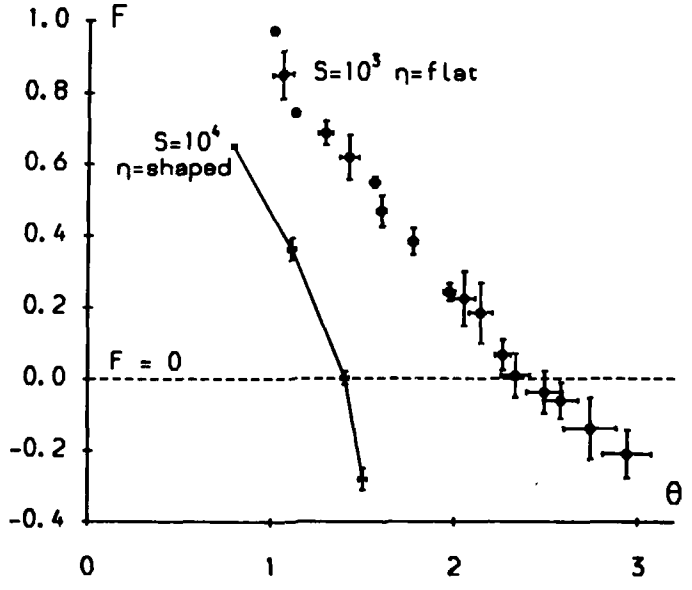

Fig.2 F vs. θ in the steady state. Bars show fluctuation amplitudes. (Cases: S = 10^3, η = flat and S = 10^4, η = shaped).

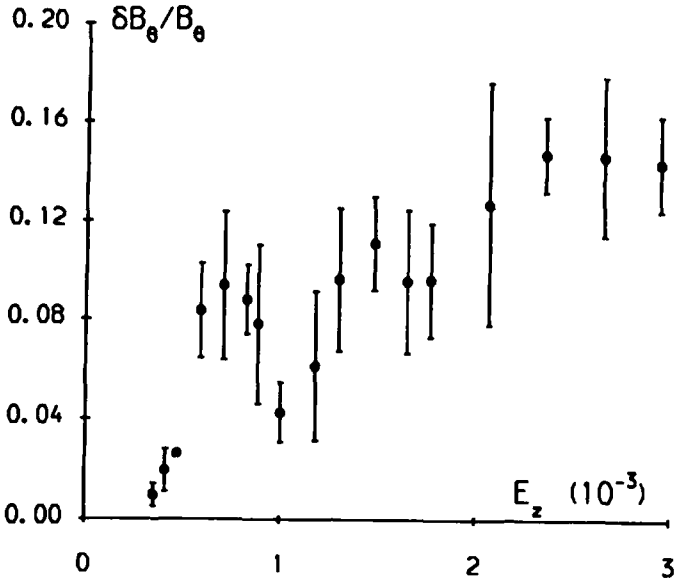

Fig.3 $\delta B_\theta / B_\theta$ vs. E_z in the steady state. Bars show fluctuation amplitudes.
(case: S = 10^3, η = flat).

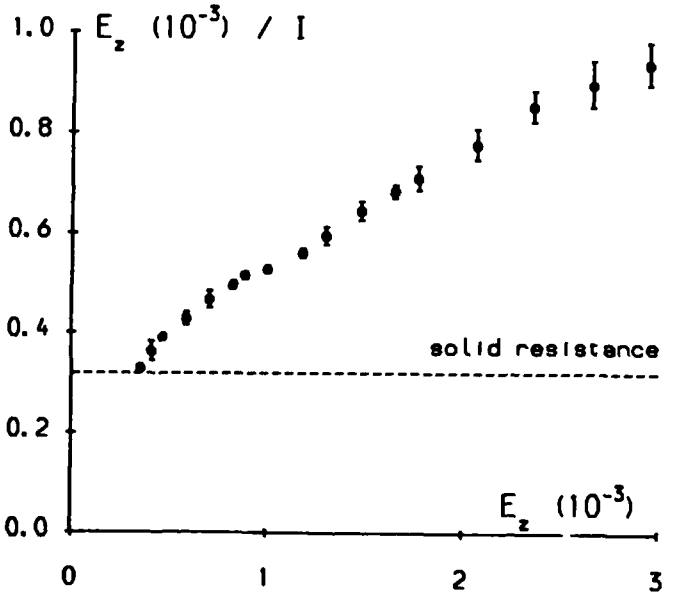

Fig.4 E_z/I vs. E_z in the steady state. Bars show fluctuation amplitudes.
(Case: S = 10^3, η = flat).

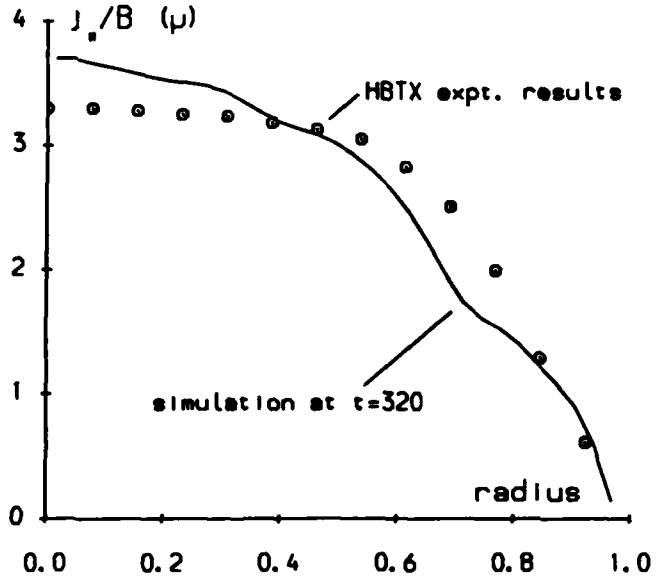

Fig.5 $j_{\parallel}/B$ vs. radius and heuristic comparison with experiment.
(Case: S = 10^3, η = flat).

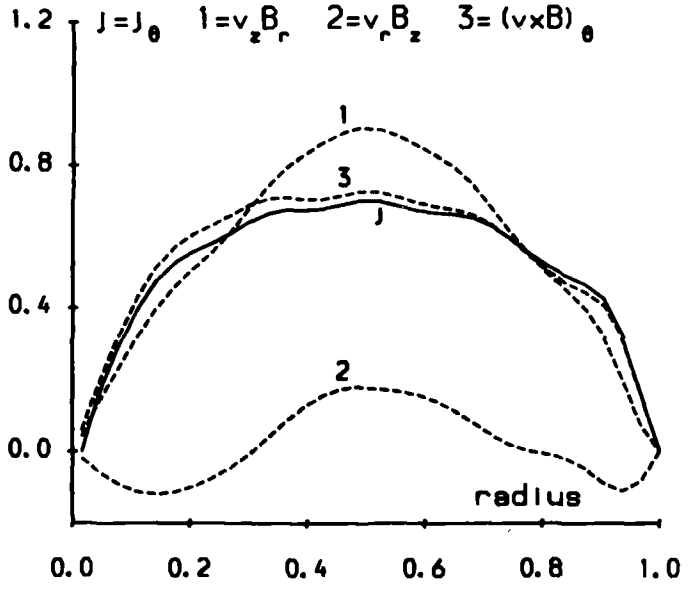

Fig.6 j_θ and (S/η) (v x $\underline{B})_\theta$ terms vs. radius.
(Case: S = 10^3, η = flat).

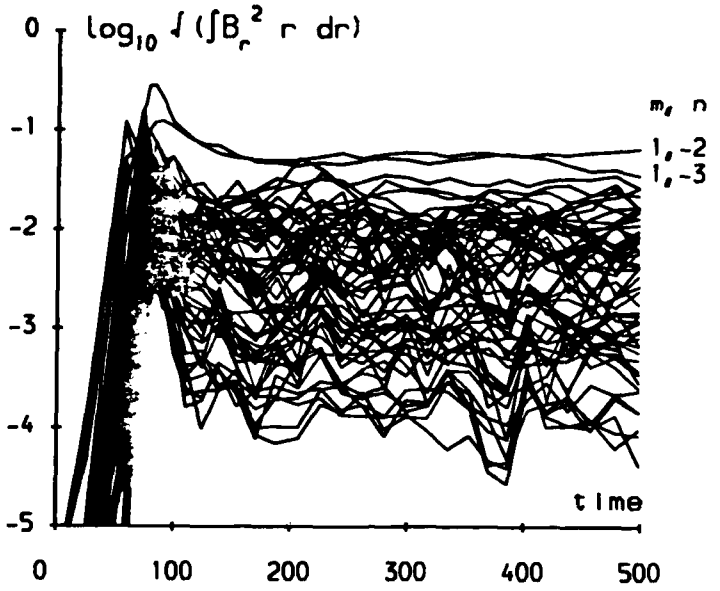

Fig.7 Energy spectrum of B_r vs. time.

(Case: $S = 10^3$, η = flat).

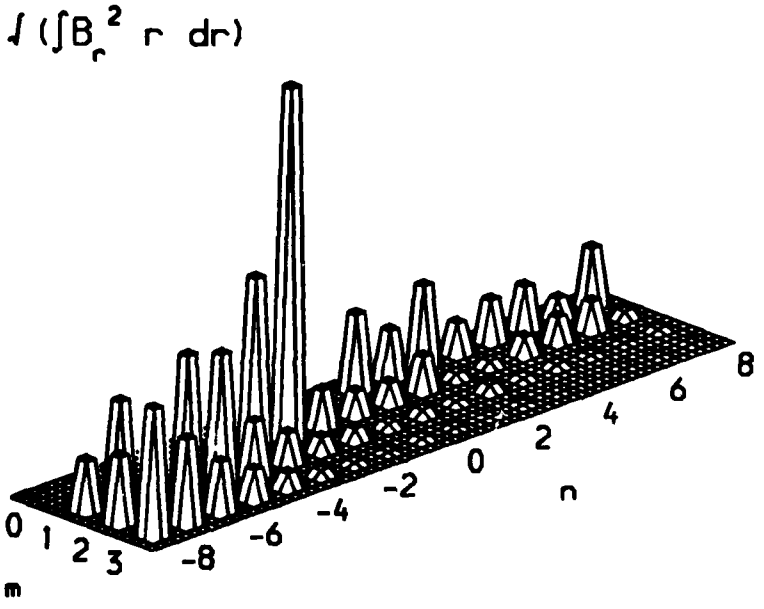

Fig.8 Energy spectrum of B_r at $t = 500$.

(Case: $S = 10^3$, η = flat).

END

DATE
FILMED
10-87